Lunar occultations events from the Earth–Moon equilateral Lagrangian point: simulations and scientific potential

A. Richichi [ID],[1]★ O. Fors [ID],[2] D. Canales [ID],[3] K. Patel,[3] L. E. Mendoza Zambrano [ID],[3] F. Criscola,[3] R. Bevilacqua,[3] S. S. Eikenberry [ID][4,5] and J. M. Gómez [ID][6]

[1]*INAF – Osservatorio Astrofisico di Arcetri, Largo E. Fermi 5, I-50125 Firenze, Italy*
[2]*Dept. de Física Quàntica i Astrofísica, Institut de Ciències del Cosmos (ICCUB), Universitat de Barcelona, IEEC-UB, Martí i Franquès 1, E-08028 Barcelona, Spain*
[3]*Aerospace Engineering Department, Embry-Riddle Aeronautical University, Daytona Beach, FL 32114, USA*
[4]*College of Optics and Photonics (CREOL), University of Central Florida, Orlando, FL 32816, USA*
[5]*Department of Physics, University of Central Florida, Orlando, FL 32816, USA*
[6]*Dept. d'Enginyeria Electrónica i Biomèdica, Institut de Ciències del Cosmos(ICCUB), Universitat de Barcelona, IEEC-UB, Martí i Franquès 1, E-08028 Barcelona, Spain*

ABSTRACT

Recently, a novel idea has been proposed to use a spacecraft orbiting closely around the L_4 or L_5 Lagrangian points of the Earth–Moon system as a vantage location for astronomical observations under unique and advantageous conditions, e.g. to investigate the Solar corona or Kordylewski clouds. In this paper, we explore the scientific advantages of this configuration to observe lunar occultations. By using simulations based on actual orbital parameters and detector performance, we find that even a telescope as small as 10 cm in a L_4 orbit would enable better light-curve sampling and higher angular resolution than from ground, and open up at the same time new spectral windows such as e.g. in the UV. We focus in particular on angular diameter measurements, which we find would be possible at the 100 μas level even at magnitudes normally considered faint in the context of ground-based LOs. Considerable benefits would also be afforded in the area of small separation binary objects, not just in terms of angular resolution but also by the capability of L_4-based observations to repeat an LO scan of a source at multiple different position angles. Additional science cases would be made possible by the high time resolution intrinsic to the LO technique and the access to UV wavelengths. On-board data pipeline codes already exist, greatly simplifying the automatic pre-processing and the data transfer requirements.

Key words: instrumentation: high angular resolution – stars: atmospheres – (stars:) binaries: general.

1 INTRODUCTION

High angular resolution is of crucial importance in understanding a large number of astrophysical phenomena, and is therefore a field in which significant technological efforts have been invested over several decades. At present, techniques such as adaptive optics (AO) and speckle interferometry (SI) are among the methods of choice for single telescopes of large to very large mirror sizes, while long baseline interferometry (LBI) is used to combine several telescopes to obtain the resolution equivalent to their ground separations. We mention also Intensity Interferometry, which has however limited sensitivity compared to LBI. These techniques are quite demanding in terms of infrastructure, of technical requirements, of computational power, and generally also in their need of calibrator sources. As a result, they are available only to specifically trained users and are often limited in application.

An interesting alternative is that of lunar occultations (LO), which was in fact the original method of choice a few decades ago. While also suffering from serious limitations, mainly in the choice of sources and in being fixed-time events, contrary to the above-mentioned techniques LOs are very easy to observe, requiring rather simple instrumentation and data analysis. Ground-based LOs have been used to study several thousands of (mainly stellar) sources, yielding hundreds of results in the area of stellar angular diameters to about 1 milliarcsecond (mas) resolution, and similar numbers of binary and multiple stars. Their potential, while not exhausted in a literal sense, has certainly already largely being exploited apart from new developments in the direction of spectroscopically dispersed LO (Shmaylova et al. 2020).

The overwhelming majority of LO observations to date have been carried out from the ground. Occultations of stellar sources have been observed, however, also from space and/or using screens other than the Moon. This is the case of the extensive body of observations of occultations by asteroids and trans-neptunian objects (TNO; see e.g. Herald et al. 2020; Ortiz et al. 2020). From space, the most outstanding example is the large set of occultations of stars by the
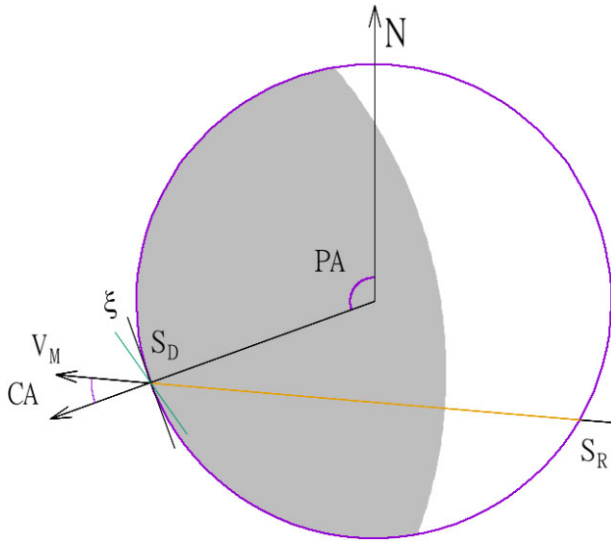
★ E-mail: andrea4work@gmail.com

Figure 1. Scheme of a LO event observed from Earth. Explanations in the text.

Saturn rings observed by the Cassini spacecraft (see e.g. Colwell et al. 2010).

In this paper, we hypothesize a spacecraft at the L₄ or L₅ Earth–Moon Lagrangian point equipped with a suitable instrument. A conceptual example of such spacecraft was initially provided by Doroba et al. (2023), and further elaborated along with a detailed study of possible orbits and associated astrodynamical parameters by Patel et al. (2023).

In this work, we investigate the possibility of carrying out an extensive program of LO observations from L₄. By this, in the paper we will implicitly intend from a spacecraft closely orbiting around L₄, not necessarily exactly on that point in a fixed position. Therefore, the distance from the spacecraft to the Moon will be slightly variable and so will be the apparent motion of the Moon. We also note that L₅ is for many aspects equivalent, and in this paper, we refer simply to L₄ to denote either one or the other. We first consider the advantages of that location in space and the basic requirements. We then present a few simulations of LO data obtained under realistic assumptions of orbital parameters and detector, and we evaluate the scientific potential of LO specifically in the area of angular diameters and small separation binary objects. Finally, we briefly list a number of other possible LO science goals.

2 LO FROM EARTH AND FROM SPACE

The LO technique consists in recording and analysing the diffraction pattern generated as the Lunar limb moves across a background source. The main geometrical quantities are summarized in Fig. 1, and a schematic example to illustrate the difference between ground-based and space-based observations, specifically from the L₄ Lagrangian point, is shown in Fig. 2. Note the considerable stretching in time of the light curves observed from L₄, which will be discussed in the following.

The defining parameters for the simulations are listed in Table 1. The distance and angular rate for the L₄ location are average values that we derived from Doroba et al. (2023). We assume that the spacecraft will be able to operate its positioning system for very brief periods to impart a rotation in the same direction as the motion of the Moon, so that the apparent rate of lunar motion is considerably

reduced. Based on papers describing attitude control of artificial satellites (see e.g. Liddle et al. 2020; Li et al. 2021), we estimate that the apparent lunar rate as seen by the spacecraft could be reduced by a factor of 5. This appears to be achievable without compromising the pointing stability, given our relatively large pixel size of 11 arcsec (see Table 2) and the short duration of the phenomenon, of order 1 s even with the temporal expansion of the fringe pattern caused by the slowdown. In the following, we highlight several differences between ground- and space-based observations, with their relative merits.

2.1 Limb irregularities

One crucial point is the assumption that the limb acts as a straight, infinite, completely opaque edge. A schematic representation of a LO event observed from the ground on Earth is shown in Fig. 1, where N denotes North, PA is the position angle of the source along the lunar limb, and V_M is the vector of lunar motion. CA is the contact angle, such that the effective rate of lunar motion is $V_e = V_M \cdot \cos(CA)$. The source crosses the limb at points S_D, S_R (disappearance and reappearance, respectively). From the ground, only dark-limb events can be observed – in this case, the disappearance. The limb may have an average local slope ξ, typically within $\pm 10°$, that must be added to CA to obtain a correct fit of V_e.

Extensive observational experience has shown that this scheme works well in the majority of cases. However, there are also several examples of light curves where an obvious departure from the straight edge hypothesis has been remarked. This seems to occur more frequently when a large integrating aperture, that is telescope diameter, is employed (Richichi & Glindemann 2012). This scenario is consistent with larger telescopes sampling different scales of lunar limb irregularities, and at the same time providing light curves with higher signal-to-noise ratio (SNR) that are more sensitive to departures from the standard model.

An instrument hosted on a spacecraft such as the one that we hypothesize here will typically be coupled to a telescope with size of ≲ 50 cm, which thanks to its small size projected at the lunar limb will be essentially free of this particular limitation.

2.2 Wavelength issues

Diffraction is chromatic, so that LO light curves appear to unfold slower in time at longer wavelengths, as can be seen by comparing the *NUV* and R cases in Fig. 2. Incidentally, we note that in fact *NUV* from ground-based observations is an impossibility due to the properties of Earth's atmosphere.

Using multiple filters to record LO events is extremely useful, as different wavelengths can provide useful complementary information on the nature of the occulted source. Examples are stars with a circumstellar envelope, or binaries in which the components are of different spectral types.

LOs have been carried out from the ground for a very large number of sources, from visual to infrared wavelengths (Richichi et al. 2012, 2014). In the visual, the limit has been usually the *V* or the *B* filter. Shorter wavelengths than this have been hampered on one side by the transmission of our atmosphere, and on the other side by the fact that LO chromatic nature would require much faster sampling with detriment on the SNR.

In space, this limitation would vanish so that enabling LO observations in the *NUV* would extend for the first time milliarcsecond resolution to this important spectral region.

2.3 Signal noise

A crucial advantage of space-based LO observations is the drastic reduction in signal noise. From Earth, the main components of noise are the detector noise, the photon shot-noise, and the scintillation noise produced as the signal travels through the Earth's atmosphere. The latter can amount to few per cent up to tens of per cents of the signal, depending on wavelength and atmospheric conditions – in particular on the ratio squared of the so-called Fried's parameter and the telescope size. Thus, it affects particularly smaller telescopes, and being proportional to the source intensity it is a major limitation for bright sources (Osborn et al. 2015). Obviously, scintillation noise is zero when no atmosphere is present as e.g. from L_4.

The remaining contributions are from the detector, and the unavoidable photon shot-noise. Their relative importance will depend on detailed mission choices, among them the telescope mirror size and the detector characteristics.

2.4 Sky coverage and brightness profiles

As seen from Earth, the Moon moves in a narrow strip of the sky, the so-called Zodiacal belt. This orbit slowly progresses at each Lunar period and eventually repeats itself with an 18.5 yr cadence, the so-called Saros cycle well known to eclipse observers. After adding parallax effects depending on the observer's position on Earth, only about 10 per cent of the sky is subject to LO. One would hope that from an observer's location at L_4 this coverage could be significantly extended. In fact, the Lagrangian points are co-planar with the Earth–Moon orbit. Even by introducing small wobbles due to the orbit of the spacecraft around L_4 (Doroba et al. 2023), the situation does not change significantly and we are left with essentially the same sky coverage as seen from Earth.

However, two very important advantages must be highlighted, while keeping in mind that LO are intrinsically one-dimensional scans along the line of motion of the Moon over the background source. These scans can be used for a parametric analysis (e.g. the diameter of a source, or the projected separation of a binary), or be converted into 1D brightness profiles (Richichi 1989). If several such 1D profiles can be gained, however, one can attempt a tomographic 2D reconstruction. From Earth, this is usually afforded only by organizing campaigns to observe the same LO from significantly different locations (see e.g. Richichi et al. 2017, α Tau).

From L_4, the situation can be more advantageous, for example by fine-tuning the details of the orbital wobbles around the Lagrangian point so that the Moon appears to cover the target source several times, most likely at different position angles, as schematically represented in Fig. 3. From Earth, LO typically occur on one side only of the Lunar disc. This is the side in darkness, while the side which is sunlit is impractical due to the very high background. Doroba et al. (2023) have shown that from L_4, almost complete darkness can be realized on two sides of the Lunar disc for several hours, sufficient for double recordings of the same event at different position angles. If during this time more than one lunar passage occurs, a corresponding number of events can be recorded. In Fig. 3, we show a case with two disappearances and two reappearances, leading to four 1D scans along different position angles, which can be used for an initial tomographic reconstruction of the source profile.

3 INSTRUMENT

From the previous considerations, we set as minimum requirements for the space-born instrument to be operational within *NUV* and *R*

bands, and to achieve millisecond sampling time with the lowest possible detector noise.

The *NUV* band ([210,280] nm) is close enough to the optical to use the same optics and focus, and a single CMOS detector can be used for e.g. *NUV* and *R* bands. In Section 5, we stress out the scientific bonus to investigate also the *FUV* [153,171] nm band. However, this band requires significantly different optics and focus specifications compared to *NUV* (Scowen et al. 2018). This can be achieved using a dichroic and a dual-arm design with two separate detectors, but this solution would be more expensive in terms of hardware and payload, and we do not envision it at the moment.

Regarding the telescope, a 10 cm diameter seems very easy to accommodate within a standard small spacecraft model such as CubeSat. For the sake of our discussion we also consider the case of a 50 cm diameter, probably only possible within the framework of an expensive, multiple-agency mission. For both cases, we assume an *F*/2 mirror.

In Table 2, we list a particular back-illuminated CMOS solution, based on the GSENSE400BSI[1] sensor. This encompasses high quantum efficiency (QE) on both *NUV* and optical bands, and shows very low readout and dark noises. The exposure range is wide enough to observe LO events within a broad range of magnitudes.

Using the detector parameters of Table 2, we compute the values of SNR as a function of stellar magnitude for a point source and a detector integration time (DIT) of 1 ms, made possible by reading out a small 128 × 128 pixels subframe largely sufficient for our purpose. The values are shown in Fig. 4 for the *NUV* and *R* filters, respectively, as specified in Table 1. Note that in our computations we used a stellar effective temperature $T_{eff} = 10\,000$ and 3500 K for the *NUV* and *R* cases, respectively. We have considered only dark limb events.

The SNR computation was performed taking into account the photon noise from the source, the read-out and dark noises, and including the detector QE and the pixel size in connection with the Airy disc of the specific telescope. There is no scintillation noise due to the absence of an atmosphere, and we neglected the photon noise from the background. This latter is due to the thermal emission from the lunar surface, and we assume it to be negligible under dark limb conditions both in the *NUV* and *R* bands with the short DIT of our application. We also do not include the small decrease in integrating area due to a secondary mirror.

Another assumption we make is that the telescope jitter is negligible. Jitter would result in a modulation of the signal, possibly of a random nature, akin to a form of noise. With the chosen focal length of 0.2 m, the specified pixel size corresponds to about 11 arcsec on the sky. The Airy disc in the *NUV* and *R* bands is 10 to 24 times smaller than this, respectively. As long as the jitter is below a few arcsecs during the few seconds of LO acquisition, we are justified in this initial assumption.

The assumptions detailed so far have been used for our simulations pertaining mainly the LO performance described in Section 4. Other applications such as those described in Section 5 might need different settings in terms e.g. of a larger field of view (FOV) at the expense of a slower, but still acceptable, DIT.

4 MAIN SCIENCE DRIVERS

In order to evaluate the scientific potential of observing LO from L_4, we need to take into account both the expected SNR as shown in
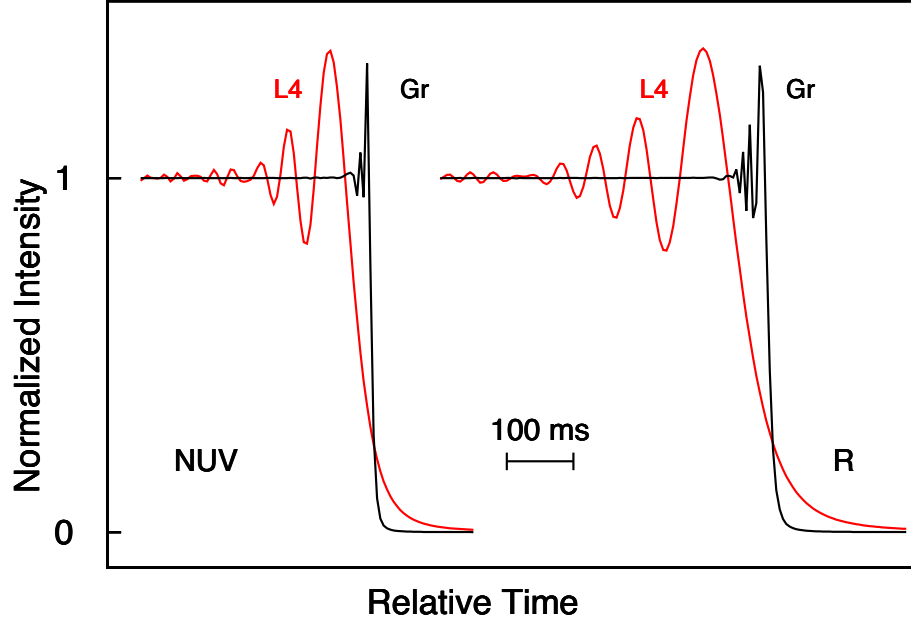
---

[1] https://www.gpixel.com/

Figure 2. Simulated LO diffraction patterns as seen from the ground on Earth and from the L₄ Lagrangian point (Gr and L4, respectively). The cases of an *NUV* and of an R filter are shown. Refer to the text for a breakdown of the simulation conditions, and for a discussion of the benefits of the L₄ vantage point.

Table 1. List of parameters used for Fig. 2.

Parameter	Earth	L₄
Telescope primary	2.5 m	0.13 m
Telescope secondary	0.9 m	–
Moon distance	384 000 km	453 000 km
NUV filter (λ_{on}, λ_{off})	210-280 nm top-hat	
R filter	SDSS *r'*	
Source T_{eff}	13 000 K	
Light curve sampling time	5 ms	
Detector integration time	1 ms, uniform	
Lunar limb rate	0.74467 m ms^{-1}	0.67884 m ms^{-1}
Counter-spin factor	1x	5x
Effective lunar limb rate	0.74467 m ms^{-1}	0.13577 m ms^{-1}
Effective lunar limb rate	0.40000 mas ms^{-1}	0.06180 mas ms^{-1}

Table 2. Features of intended CMOS for *NUV* and R bands.

Parameter	Value
CMOS sensor	GSENSE400BSI-TVISB
Format, pixel size	2k × 2k, 11 μm
NUV sensor QE	79 per cent peak at 240 nm
	28 per cent peak at 210 nm
	29 per cent peak at 280 nm
R sensor QE	93 per cent peak at 620 nm
	95 per cent peak at 570 nm
	76 per cent peak at 740 nm
Full well capacity (e$^-$)	HDR: 80,000 ; STD: 100,000
Readout noise	High Gain e$^-$: 1.6(med) / 1.7(rms)
Dark current (e$^-$/s/pix @50°C)	0.5
Dynamic range	62500:1
Bit depth	16bit & 12bit

Figure 3. Scheme of multiple LO for a same source observed from L₄.

different orbital choices. For our present discussion, we consider two orbits around L₄, namely SPO1 and SPO3 in the above paper, which we have adapted into our Fig. 5. These orbits encompass the possible range of lunar limb rates, with average values of 0.050 and 0.473 arcsec s^{-1} respectively, and distances to the Moon quite comparable to those in ground-based LO. For comparison, ground-based LO have typical limb rates of 0.4 arcsec s^{-1}. After including counter-spin as discussed in Section 2, the limb rates as observed from the spacecraft during a LO event would then be ≈0.01 and 0.1 arcsec s^{-1}, respectively, or about 4–40 times slower than from Earth. This does not include the additional decrease in limb speed, at L₄ as well as from Earth, due to contact angle as discussed in Section 2.1.

Fig. 4, and the effective lunar limb rate which in turns determines the light-curve sampling. An example of a limb rate was given in Table 1, while detailed computations are reported in Patel et al. (2023) for
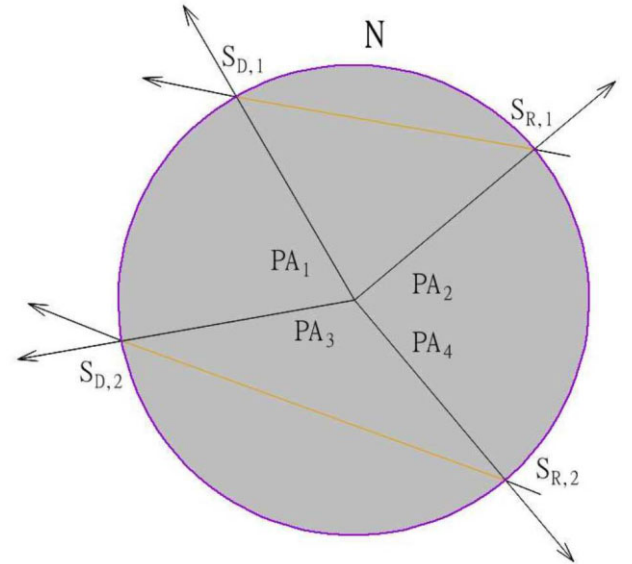
Downloaded from https://academic.oup.com/mnras/article/527/3/6616/7453664 by guest on 08 February 2024
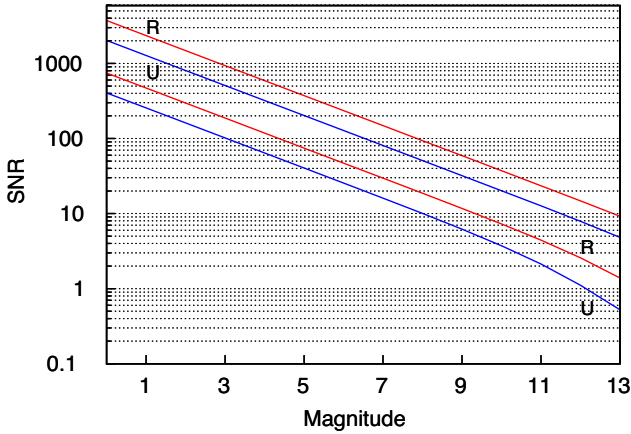
Figure 4. Estimation of SNR as a function of stellar magnitude for a point source with the detector parameters listed in Table 2 and according to the discussion in Section 3. The two top curves are for a telescope mirror diameter of 50 cm in the *R* and *NUV* filters. The two bottom curves are for a 10 cm mirror. Detector integration time is 1 ms in all cases.
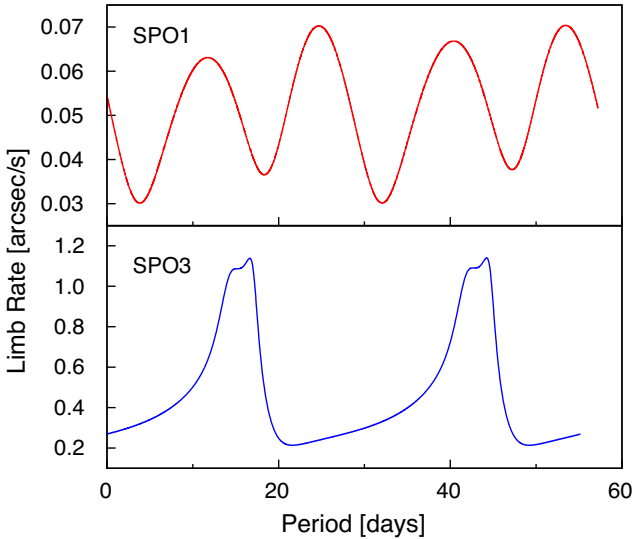

Figure 5. Nominal lunar limb rate as seen from two possible orbits of a small spacecraft around L_4. Adapted from Patel et al. (2023), where full details are given.

Also note in Fig. 5 the marked asymmetry of the SPO3 orbit, in which the limb rate is in fact below the average value for 2/3 of the orbital period. Given the significant difference in limb rates, we use DIT of 1 ms for the faster SPO3 orbit, but we use a slower DIT of 5 ms for the SPO1 case, thereby increasing the SNR with respect to the values in Fig. 4. After including read-out, we assume actual sampling times of 2 ms for SPO3 and 7 ms for SPO1. The parameters that we adopt for our simulation of the LO science are summarized in Table 3.

4.1 Angular diameters

We start with one of the main science cases for LO, namely the measurement of angular diameters. This is the key to measure effective temperatures, which are in turn one of the few observational checks available to compare models of stellar atmospheres and energy production. Thanks to ground-based LO and by now also

Table 3. Adopted parameters for the chosen bands, detector, and orbits as discussed in the text.

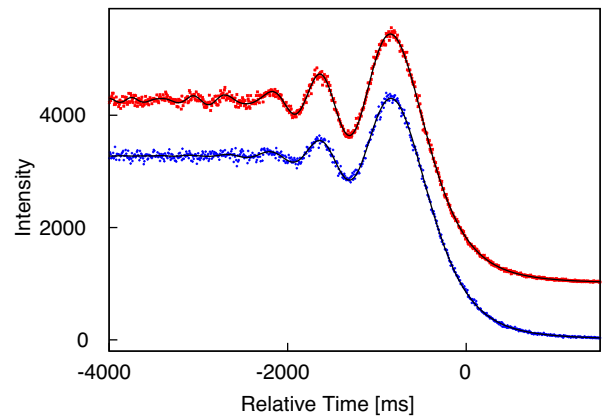| Orbit	SPO1	SPO3
Min. limb rate (arcsec s^{-1})	0.0301	0.2139
Max. limb rate (arcsec s^{-1})	0.0703	1.1400
Aver. limb rate (arcsec s^{-1})	0.0503	0.4727
After counter-spin (arcsec s^{-1})	0.01	0.1
DIT (ms)	5	1
Sampling time (ms)	7	2
SNR mag$_{NUV}$ = 1	571	256
SNR mag$_R$ = 1	1051	470
SNR mag$_{NUV}$ = 8	23	10
SNR mag$_R$ = 8	42	19
Limit mag$_{NUV}$ SNR = 3	12.1	10.4
Limit mag$_R$ SNR = 3	13.5	11.7

Figure 6. LO light curves (dots) and best fits (solid line) for a point source (top, offset by 1000) and a 2 mas uniform-disc diameter source (bottom), both with mag$_{NUV}$ = 6 and added noise according to the details in Section 4.1. The intensity is measured in photoelectrons generated with DIT = 5 ms. Note the difference in contrast between the two cases in the higher order fringes.

LBI, such data are widely available for cool giant stars which exhibit diameters of few to tens of mas. For what concerns hotter stars and especially main-sequence stars, however, the requirement is to resolve sub-mas diameters and such data are still relatively scarce.

The noiseless LO diffraction patterns for a point-source in the *NUV* and *R* filters were shown in Fig. 2. In Fig. 6, we show the diffraction patterns simulated for a point-source and for a 2 mas uniform disc (UD) diameter source, in the case of a LO observed from the SPO1 orbit and the Moon at 4×10^5 km. In both cases, mag$_{NUV}$ = 6. With the assumed 5 ms DIT, the expected photoelectrons rate and SNR on the unocculted signal are 3266 and 57, respectively. It can be appreciated how the decrease in fringe contrast, as expected for a resolved angular diameter, is easily detected even at this relatively faint magnitude and small UD value. A comparison with ground-based LO is not possible, since the *NUV* band is not accessible from there, but the numbers already compare favorably with measurements done with much larger telescopes on Earth at longer wavelengths (see e.g. Richichi et al. 2014, and references therein). For illustration, in this specific example the difference between the output parameters from the fit to the simulated curve with added noise and the input parameters amounts to +0.4 per cent (limb rate), +0.1 per cent (intensity), −0.3 per cent (angular diameter).

Table 4. Smallest UD angular diameter measurable as a function of stellar magnitude, under the conditions discussed in Section 4.1.

mag	UD (mas)	SNR[a]	SNR[b]
	NUV, SPO1, DIT = 5 ms		
5	0.35 ± 0.05	111	91
6	0.45 ± 0.05	72	57
7	0.70 ± 0.05	42	36
8	0.65 ± 0.10	27	22
9	1.25 ± 0.05	18	14
10	1.35 ± 0.15	11	9
	R, SPO3, DIT = 1 ms		
4	0.40 ± 0.10	140	118
5	0.65 ± 0.05	93	75
6	1.10 ± 0.05	57	47
7	1.10 ± 0.10	36	30
8	0.80 ± 0.20	22	19
9	2.10 ± 0.15	14	12
10	2.00 ± 0.30	9	7

[a]SNR of the fit to the diffraction pattern.
[b]SNR of the unoccluded source signal.

We have carried out simulations to investigate the capability to resolve angular diameters as a function of stellar magnitude in the *NUV* band and *R* bands, according to the SNR computations already presented. In the *NUV*, we have assumed the SPO1 orbit and used 5 ms, 7 ms, 10 cm, 10 000 K for the DIT, the sampling time, the telescope diameter and the source effective temperature, respectively. In the *R* band, we assumed the SPO3 orbit and the same parameters above were set at 1 ms, 2 ms, 10 cm and 3500 K. In both cases, the spacecraft-Moon distance is 4×10^5 km, the orbital speeds include counter-spin and the events are on the dark limb.

The smallest angular diameters that can be resolved by LO observed from L$_4$ under the above conditions are listed in Table 4. By this, we mean a value such that any smaller diameter would result in a light curve undistinguishable from that of a point source, under the given SNR. The values should be considered only indicative as we used single simulations rather than the computational intensive Montecarlo approach. The table lists two SNR values: the first one is derived from the fit to the simulated light curve, while the second one is the value extracted from Fig. 4 and refers to the unoccluded stellar signal only. As the former has less noise on the occulted part of the light curve, it is expected to be consistently higher than the latter.

Note that in Table 4 we cut off the brighter magnitudes. The reason is that our software was originally designed to deal with milliarcseconds, rather than microarcseconds, diameters so that simulations for objects smaller than ≈0.3 mas might not be free from numerical errors. Indications are, nevertheless, that angular resolution at the ≈ 100 μas level can be achieved for bright magnitudes. This would open up the possibility to measure not just diameters and effective temperatures with extremely high accuracy, but also allow us to study deviations from the standard UD hypothesis and investigate second-order effects due to limb-darkening and photospheric spots.

4.2 Binary sources

A second main application of the LO technique has traditionally been the investigation of small separation binary or multiple sources, including not just stars but also e.g. asteroids. This has been done either by dedicated studies on specific objects (e.g. Dyachenko et al. 2021) or by serendipitous discoveries (e.g. Evans et al. 1986, and previous papers in the series). Using a sample of over 1000 light
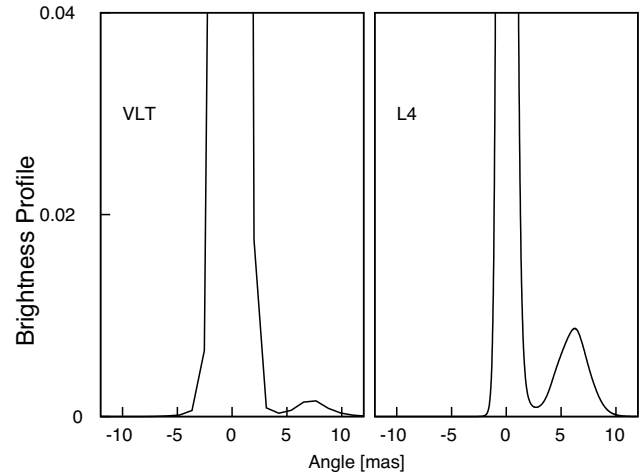

Figure 7. Normalized brightness profile for IRAS 17371-2207, discovered as binary by Richichi et al. (2013). *Left:* Original result from a LO recorded at the ESO VLT in *K* band. *Right:* Result from simulated data for a LO recorded in *R* band at L$_4$, using the same source parameters and equivalent noise to the original observation. In the former case, the secondary is separated by six resolution elements, in the latter by about 300. See the text for details, including the apparent difference in brightness ratio between the two cases.

curves recorded at the ESO VLT in the near-infrared, Richichi et al. (2014) have concluded that about 8 per cent of LO events of random field stars resulted in binary star detections, typically new discoveries, with separations often below the 0.01 arcsec level.

The first important advantage of detecting binary objects by LO at L$_4$ is the significant slow-down of fringe frequency with respect to ground-based observations, as already illustrated in Fig. 2.

This effect is the same for both of the binary component, so it does not lead to an obvious better separation of the fringe patterns for the untrained eye. However, it does lead to a much better sampling so that the resolution and errors on angular separation in a computer algorithm are significantly improved.

We have taken as an example the source IRAS 17371-2207, discovered as binary by Richichi et al. (2013) with projected separation 6.2 mas and 3.71 mag difference, from a LO recorded at the ESO VLT in the *K* band. The resulting brightness profile, yet unpublished in graphical form, is shown in the left panel of Fig. 7. We have simulated a light curve in the *R* band for two components with the same separation and brightness ratio as in the original paper, and the same noise level. For this, we have adopted the average limb rate on SPO1 after counter-spin (see Table 3), with DIT and sampling of 1 and 2 ms, respectively. The result is shown in the right panel of Fig. 7. The secondary component is detected with similar separation as expected, but in the original VLT data this amounts to 6 resolution elements, while in the simulated L$_4$ data the two components are separated by 310 resolution elements. This implies, in turn, that under the same conditions, L$_4$-based LO observations have the potential to resolve secondary components up to ≈50 times closer in to the primary then ground-based LO, or separations close to the 100 μas level.

Note that the relative intensity of the secondary peak appears quite different in the two cases of Fig. 7. This is due to the reconstruction algorithm, described in Richichi (1989), which is regulated by resolution elements and standard deviation in the fit to the fringes which in turn are different in the two cases.

In parallel, the absence of background noise translates, as was the case for our discussion on angular diameters, to impressive sensitivity

for the small telescope size considered, and in particular it enables the detection of companions with a larger magnitude difference from the primary than from Earth under comparable conditions.

One more crucial advantage of L_4-based observations is the ability to repeat a LO at different position angles (see Fig 3). This would effectively remove the limitation of projected separations only, and lead to real separations that are needed e.g. for detailed studies of orbits and temporal evolution of binary systems.

5 ADDITIONAL SCIENCE GOALS

In addition to the relatively standard LO applications of measuring angular diameters and binary or multiple sources, in our case with a very high level of sensitivity and angular resolution, there are several additional science goals that can be addressed in principle. In the following we will restrict ourselves to the *NUV* and *R* bands already considered previously, but we note that more bands are available with the same detector. We choose this approach to show what can be done with the cheapest possible instrument design having one detector only. However, should the mission budget afford the expense, we remark that adding a *FUV* capability, such as via a dichroic 2-beam design including two detectors, would significantly increase the scientific rewards. For example, the FUV would allow us to measure in more detail the stellar chromospheric emission in comparison to the photosphere for some selected stellar types (see e.g. Section 5.3). Also, two detectors would enable simultaneous observations in UV and optical, again with distinct advantages for the science goals listed in the following.

5.1 Lunar impacts flashes

The planned spacecraft would observe the lunar dark limb from L_4 almost continuously, as discussed later in Section 6. Our chosen detector has 2k × 2k pixels, corresponding to a FOV large enough to encompass the whole limb if so chosen, possibly at a slightly reduced read-out rate but still in the sub-second range. This opens up the opportunity to record serendipitously lunar impacts flashes (LIF) in two bands (*NUV* and *R*) for the entire length of the mission. Our LIF observations would be of great interest in the context of the Earth–Moon Space Situational Awareness, especially for ∼dm-sized debris or natural meteoroids in the cislunar environment. LIF have been monitored from ground by NELIOTA programme since 2017 (Liakos et al. 2020). Our observations would complement the monitoring of LIF as will be conducted by the CubeSat Lunar Meteoroid Impacts Observer (LUMIO; Topputo et al. 2023), which will operate in optical and NIR.

5.2 Rings and prominences in the solar system

Apart from the four solar system planets known to have rings, very few dwarfs planets and minor bodies have been detected to host such structures, which are a key information for the understanding of the planetary formation. The number of such detections is slowly increasing with the combination of ground-based and space-based planetary occultations, i.e. the occulting body is not the Moon but the Solar System body we want to study. A few known examples are the Centaurs Chiron (Ortiz et al. 2023), Chariklo (Braga-Ribas et al. 2014), the dwarf planet Haumea (Ortiz et al. 2017), and the TNO Quaoar (Morgado et al. 2023).

It is possible in principle, although we did not check by simulations, that ring systems similar to those mentioned above could be resolved by means of planetary occultations seen from L_4, if the occulted star is bright enough, by reducing the time sampling to get

a higher SNR. A challenge is that the intrinsic widths of the rings might not suffice for a deep enough dip. However, we note that the detection of Quaoar rings by CHEOPS (30 cm aperture) was with coarse time sampling (∼ 4 s). In our case, the comparison of contrast in *NUV* and *R* light curves would significantly help to differentiate real signals from noise features.

Another potential science case in the same category is to detect by LO from L_4 prominences in moons of the Solar System giants. Some examples of these phenomena are Enceladus south polar geysers, sourcing the icy particles of the Saturn E ring (Postberg et al. 2023), and putative water plumes rising above Europa crusted ocean (Jia et al. 2018). The LO detection of these prominences in cold environments would be enhanced in *NUV* band. Being giants moons it should not be a problem to reach the necessary SNR, and time resolution could be slowed down if necessary while keeping the required angular resolution.

5.3 Star spots maps and stellar variability

With the advent of precise space-based exoplanetary transits (JWST, CHEOPS), the characterization of stellar variability during the transit is one of the largest pitfalls that precludes deriving other measurements (e.g. planetary atmospheres) more accurately. A few photometric and spectroscopic observations just before and after a given transit might provide a very short-term insight of the stellar variability, but are far from providing a detailed picture.

The 1–5 ms time resolution of our proposed mission would allow us to achieve the angular diameter resolution at the level of ≈ 100 µas for stars brighter than ∼8.5 mag and SNR ≥ 20. Such high angular resolution would enable to physically characterize the stellar variability with phenomena such as limb-darkening, spots, faculae, and their temporal variation in optical and *NUV* wavelengths, if a baseline of some days is used. For this, repeated observations within periods shorter than the variability are needed, which could be possible depending on the details of the orbit around L_4.

This effort of obtaining a map of stellar spots would be a step forward with respect to other studies, such as those based on purely analytical physical models (Herrero et al. 2016) or on machine-learning using physical observables (Perger et al. 2023). The unprecedented addition of the *NUV* band will be crucial, since there the contrast of spots versus photosphere and chromosphere is enhanced, especially for the M-dwarfs. We note that LO allow to reconstruct model-independent brightness profiles (Richichi 1989) of arbitrary complexity, as needed for studies of stellar surface structures.

5.4 Search of disks around young and nearby stars

The study of discs around young stars has recently gained high interest, since it is now understood that they are the cradle of planetary formation. Initial investigations by LO and speckle interferometry revealed a large number of discs and envelopes around T Tau and Herbig Ae/Be stars in the solar neighbourhood (see e.g. Leinert et al. 1991; Simon et al. 1995; Leinert et al. 2001, and references therein). More extended, cooler discs are now regularly resolved at submillimetre wavelengths. The case of HL Tau has become paradigmatic (ALMA Partnership 2015). Outer and intermediate parts of the HL Tau disc were measured to be 0.075 and 0.025 arcsec, respectively. These parts of the disc are not visible in *R* and *NUV*, but the sensitivity and SNR of LO from L_4 could potentially resolve more interior, hotter parts of the disc. We note that two nearby star-forming regions, namely Taurus-Auriga and Ophiuchus-Scorpius, are regularly occulted by the Moon from Earth and they will be from L_4 as well.

6 DISCUSSION AND CONCLUSIONS

Through our simulations, we have proven that observing LO from a spacecraft orbiting around L_4 could lead to a great improvement in angular resolution and sensitivity compared to the ground-based case. It would also open up completely new spectral windows such as in the UV, where such observations are not possible at all from the ground. In turn, this would significantly advance our understanding of stellar physical parameters for single stars, binary and multiple stars, and their surface and circumstellar characteristics. We have also considered several additional science cases which would benefit greatly from LO measurements in *NUV* and optical from L_4.

Naturally, a L_4 spacecraft will have other science goals in addition to LO observations. Patel et al. (2023) mention e.g. the study of the Solar corona and of Kordylewski clouds, subjects which will be expanded in separate papers (in preparation). At this point, we do not know the exact repartition of time dedicated to one science goal or the other, but we note that e.g. coronographic observations will take place during a total solar eclipse from L_4 which, depending on the details of the orbit, should occur only once or very few times per month and last of order of a few hours. LO, on the other hand, can be observed any time of the month except for possibly 1–2 d around the L_4 full moon phase. By their nature, in addition to targeted observations of selected sources LO are also ideally suited as time filler observations, making the mission productive close to 100 per cent of its lifetime.

To provide a context, we have estimated the number of stars subject to LO in *R* band from the SPO3 orbit with an expected detection SNR of 3 (cfr. Table 3) to be of order 15 millions, over the whole 18.5 yr lunar cycle. Even by decreasing this number using a realistic mission lifetime of few years, we would still be provided with an an almost infinite reservoir of potential LO targets. In practice, however, we expect that a considerable amount of time could be dedicated to alternative science goals such as those of Section 5, or pertaining the Solar corona.

We have also demonstrated how the goals of the mission could be accomplished even with a relatively small telescope: for our simulations we have used a 10 cm mirror, which could be fitted on commercially available satellites such as CubeSat. We also note that the data flow to Earth would be relatively easy to manage even at low transmission rates by using on-board pipelines which are largely already existing. In particular, we plan to run a first pipeline using optical and *NUV* images, performing an automatic astrometric reduction with SExtractor (Bertin & Arnouts 1996) and Astrometry.net (Lang et al. 2010). In a second pipeline, each LO 3D FITS cube will be extracted into a 1D light curve. This task will be automatically performed by the specifically designed Automated Wavelet-based Lunar Occultations Reduction Package (AWLORP; Fors et al. 2008), which allows to calibrate the 3D cube, to extract the light curve and, thanks to the wavelet transform properties, to efficiently compute initial guesses of the parameters of the light-curve fit. Allowing for several seconds of light curve with 1 ms sampling and 16-bit accuracy, we expect $\sim$100 kB which could be further significantly reduced by compression. Even in the case of continuous LO observations, which we assume will be of order once every 2 min to account for source acquisition and data storage, we will be dealing with a flow of $\sim$1 MB per hour. On the ground, a full suite of light curve analysis programs is already developed and available.

Although a large number of factors still need to be evaluated and demonstrated, such as e.g. the required attitude and tracking accuracy

of the spacecraft, its power requirements and its lifetime, we believe that the proposed mission is in principle well feasible and within the budget of a typical low-cost space project.

DATA AVAILABILITY

There are no new data associated with this article.

REFERENCES

ALMA Partnership, 2015, ApJ, 808, L3
Bertin E., Arnouts S., 1996, A&AS, 117, 393
Braga-Ribas F. et al., 2014, Nature, 508, 72
Colwell J. E. et al., 2010, AJ, 140, 1569
Doroba S. et al., 2023, 33rd AAS/AIAA Spaceflight Mechanics Meeting. Austin, Texas (AAS 23-326)
Dyachenko V. et al., 2021, MNRAS, 508, 273
Evans D. S. et al., 1986, AJ, 92, 121
Fors O. et al., 2008, A&A, 480, 297
Herald D. et al., 2020, MNRAS, 499, 4570
Herrero E. et al., 2016, A&A, 586, A131
Jia X. et al., 2018, Nat. Astron., 2, 459
Lang D. et al., 2010, AJ, 139, 1782
Leinert C. et al., 1991, A&A, 250, 407
Leinert C. et al., 2001, A&A, 375, 927
Li L., et al, 2021, Chin. J. Aeronaut., 34, 191
Liakos A. et al., 2020, A&A, 633, A112
Liddle J. D. et al., 2020, Nat. Astron., 4, 1026
Morgado B. E. et al., 2023, Nature, 614, 239
Ortiz J. L. et al., 2017, Nature, 550, 219
Ortiz J. L. et al., 2020, The Trans-Neptunian Solar System. p. 413, Elsevier, Amsterdam
Ortiz J. L. et al., 2023, A&A, 676, L12
Osborn J. et al., 2015, MNRAS, 452, 1707
Patel K. et al., 2023, Acta Astron., 211, 781
Perger M. et al., 2023, A&A, 672, A118
Postberg F. et al., 2023, Nature, 618, 489
Richichi A., 1989, A&A, 226, 366
Richichi A., Glindemann A., 2012, A&A, 538, A56
Richichi A. et al., 2012, ApJS, 203, 33
Richichi A. et al., 2013, AJ, 146, 59
Richichi A. et al., 2014, AJ, 147, 57
Richichi A. et al., 2017, MNRAS, 464, 231
Scowen P. A. et al., 2018, Proc. SPIE, 10699, 106990F
Shmaylova E. et al., 2020, Res. Astron. Astrophys., 20, 176
Simon M. et al., 1995, ApJ, 443, 625
Topputo F. et al., 2023, Icarus, 389, 115213

This paper has been typeset from a TEX/LATEX file prepared by the author.